PCCP

^{15}N and ^{2}H NMR relaxation and kinetics of stepwise double proton and deuteron transfer in polycrystalline tetraaza[14]annulene

Uwe Langer,[a] Lidia Latanowicz,[ab] Christof Hoelger,[a] Gerd Buntkowsky,[a] Hans-Martin Vieth[c] and Hans-Heinrich Limbach*[a]

[a] *Institut für Chemie der Freien Universität Berlin, Takustrasse 3, D-14195 Berlin, Germany*
[b] *Institute of Physics, Plac Slowianski 6, Pedagogical University, 65-069 Zielona Gora, Poland*
[c] *Fachbereich Physik, Freie Universität Berlin, Arnimallee 13, D-14195 Berlin, Germany*

Received 18th September 2000, Accepted 16th January 2001
First published as an Advance Article on the web 22nd March 2001

We have studied the dynamics of nano- to picosecond proton transfer processes in the ^{15}N labeled polycrystalline TTAA molecule (1,8-dihydro-5,7,12,14-tetramethyldibenzo(*b*,*i*)-$^{15}N_4$-(1,4,8,11)-tetraazacyclotetra-deca-4,6,11,13-tetraene) by a combination of 9.12 MHz ^{15}N T_1 relaxation time measurements under CPMAS conditions (CP ≡ cross polarization and MAS ≡ magic angle spinning) and by 46 MHz ^{2}H T_1 relaxation time measurements of a static sample of polycrystalline doubly deuterated TTAA-d_2. By an analysis of the temperature dependent isotropic ^{15}N chemical shifts of the four inequivalent ^{15}N atoms in TTAA evidence was obtained for a network of proton transfer steps between two *trans*-tautomers 1 and 2 and two *cis*-tautomers 3 and 4 which interconvert by single proton transfers. However, in the temperature range between 100 and 400 K tautomer 4 is not formed to an observable extent. Only a single spin diffusion averaged ^{15}N T_1 relaxation time for all nitrogen atoms was observed, whereas the two deuterons in TTAA-$^{15}N_4$ give rise to two different ^{2}H T_1 relaxation times. An appropriate ^{15}N and ^{2}H relaxation theory in the presence of the reaction sequence $1 \rightleftarrows 3 \rightleftarrows 2$ was developed and used to convert the relaxation data into the rate constants including the H/D isotope effects of the two reaction steps. Some ^{15}N relaxation data obtained for TTAA at natural ^{15}N abundance allowed us to assign a larger barrier to the reaction step $1 \rightleftarrows 3$ and a smaller barrier to the step $3 \rightleftarrows 2$ which dominates the longitudinal ^{15}N and ^{2}H relaxation. The Arrhenius diagram including the kinetic isotope effects showed that tunneling is operative at low temperatures. The results are discussed in comparison to those obtained previously for related intramolecular proton transfers in porphyrin, porphycene and the related DTAA molecule (1,8-dihydro-6,13-dimethyldibenzo(*b*,*i*)-$^{15}N_4$-(1,4,8,11)-tetraazacyclotetra-deca-4,6,11,13- tetraene).

Introduction

For a number of years, longitudinal ^{1}H and ^{2}H NMR relaxometry has been used to follow the kinetics of fast proton[1–6] and deuteron transfer[7–10] in organic solids. This is possible because these processes modulate homonuclear proton dipolar and deuteron quadrupolar interactions. In the simplest cases, two tautomeric states 1 and 2 need to be considered, which interconvert by proton or deuteron transfer rate processes characterized by the rate constants k_{12} and k_{21}, where the equilibrium constant is given by $K_{12} = k_{12}/k_{21}$. In order to extract k_{12} from the longitudinal relaxation times T_1 information about the equilibrium constant K is needed, besides information about the magnetic interactions modulated by the proton or deuteron transfer. In the case of single crystal studies the latter as well as K can be extracted by analyzing the temperature dependent dipolar or quadrupolar interactions.[1,8] In the case of powdered crystals the determination of equilibrium constants and, therefore, of k_{12} from T_1 measurements is more difficult. An additional difficulty arises, if more than two tautomeric states are involved in the system.

Therefore, the combination with additional techniques such as high resolution ^{15}N solid state NMR spectroscopy under the conditions of cross polarization (CP), magic angle spinning (MAS) and high power proton decoupling is desirable. Using this method it is possible to determine both equilibrium and rate constants of proton transfer from and to nitrogen, as long as this process modulates the isotropic ^{15}N chemical shifts.[11–15] Thus, even kinetic hydrogen/deuterium isotope effects of single and multiple solid state proton transfers could be followed in a wide temperature range by lineshape analysis and magnetization transfer experiments in the millisecond to second timescale.[11d,13a] A considerable extension of the method was the proposition to study and analyze longitudinal ^{15}N solid state relaxation caused by the modulation of the heteronuclear dipolar ^{1}H–^{15}N interaction during proton transfer, in combination with the determination of the equilibrium constants of proton transfer by analysis of the temperature dependent ^{15}N line positions.[15a] It was shown that the relaxation times obtained under MAS conditions are very close to the isotropic relaxation times for which the connection between the kinetics and relaxation is straightforward. As a first case the method was applied to the tautomerism of DTAA (dimethyldibenzotetraaza[14]annulene or 1,8-dihydro-6,13-dimethyldibenzo(*b*,*i*)-$^{15}N_4$-(1,4,8,11)-tetraazacyclotetra-deca-4,6,11,13-tetraene) which exhibits a double proton transfer in the solid state according to Fig. 1a.[15a] In the case of the tautomerism of DTAA and as found recently also in the case of porphycene,[15c] the observation of a ^{15}N T_1 minimum made it possible to obtain rate constants of the tautomerism in the micro- to nanosecond timescale. Extrapolation of the data to lower temperatures gave a good agreement with the rate constants obtained for DTAA in the millisecond timescale by ^{15}N CPMAS lineshape analysis.[15a]

 DOI: 10.1039/b007564g

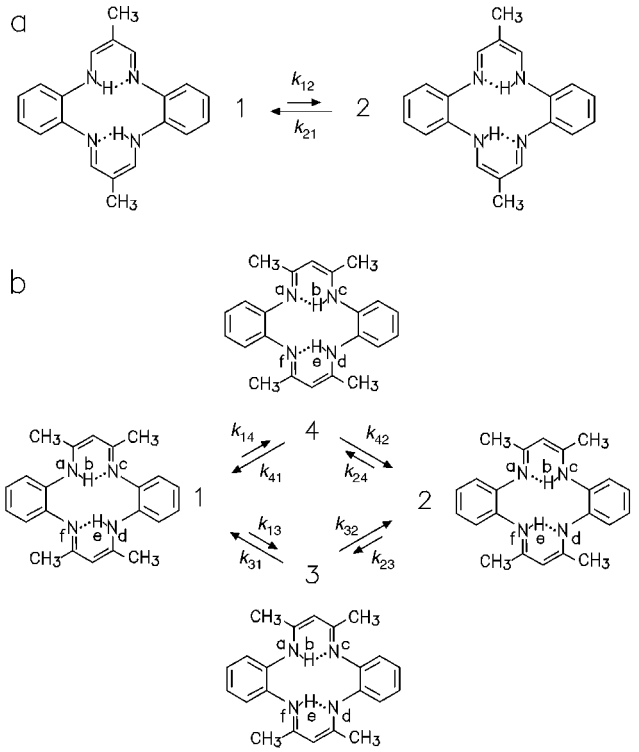

Fig. 1 The solid state tautomerism of (a) DTAA and (b) TTAA. The tautomeric states *r*, *s* are represented by arabic numbers and the nuclei *I*, *S* of the two intramolecular hydrogen bonds by latin letters. The equilibrium constants are labeled as $K_{rs} = k_{rs}/k_{sr} = x_s/x_r$, where k_{sr} are the rate constants and x_s, x_r the mole fractions. According to ref. 14(*d*), only states 1, 3 and 2 are populated between 80 and 400 K to an observable extent.

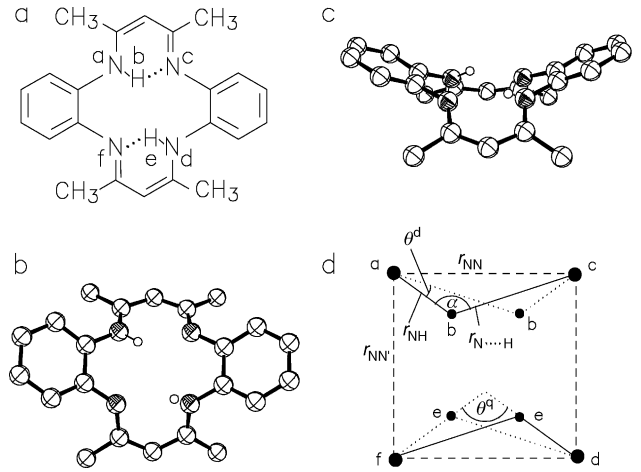

Fig. 2 (a) Chemical structure of TTAA, (b) and (c) crystal structure of TTAA according to Goedken *et al.*[16] and (d) geometries of the two intramolecular hydrogen bonds in TTAA. $\theta^{d} = \theta^{SI}_{rs}$, where *r*, *s* = 1 to 4, *S* = a, c, d, f and *I* = b, e represents the jump angle of the dipolar ^{15}N–^{1}H interaction. $\theta^{q} = \theta^{I}_{rs}$ represents the corresponding jump angle of quadrupole interaction experienced by deuteron *I*. $r_{NN} = 2.675$ Å, $r_{NN'} = 2.699$ Å. The proton locations are determined as described below.

It is clear that ^{15}N NMR relaxometry is not suitable to measure rate constants of the corresponding deuteron transfer because of the much smaller dipolar ^{2}H–^{15}N interaction. Therefore, we explore in this paper the possibility to combine ^{15}N NMR measurements of rate and equilibrium constants of proton transfer with ^{2}H relaxation measurements. Moreover, we consider also the more complex process of a stepwise double proton transfer involving more than two states. As an example, we study the tautomerism of TTAA (tetramethyldibenzotetraaza[14]annulene-$^{15}N_4$) or 1,8-dihydro-5,7,12,14-tetramethyldibenzo(*b*,*i*)-$^{15}N_4$-(1,4,8,11)-tetraazacyclotetra-deca-4,6,11,13-tetraene). The stepwise tautomerism of this molecule depicted in Fig. 1b was established by observing four inequivalent ^{15}N nuclei whose average temperature dependent proton densities leads to characteristic temperature dependent signal positions.[14] The four tautomers of the TTAA exhibit different temperature dependent mole-fractions, however, at low temperatures only form 1 was populated, and at higher temperatures also forms 2 and 3, to about a similar extent.[14d] As a result, the proton tautomerism of polycrystalline TTAA molecule can be approximated by an interconversion of three states $1 \rightleftarrows 3 \rightleftarrows 2$, *i.e.* by a proton transfer along a triple minimum potential. The changes observed are so significant that TTAA is now used as a ^{15}N chemical shift NMR thermometer.[13,14] The degeneracy of the various tautomers is lifted by intermolecular interactions. This tautomerism makes it very difficult to assign the proton locations by X-ray diffraction. The crystal structure of TTAA according to Goedken *et al.*[16] and the geometries of the two intramolecular hydrogen bonds established in this paper are depicted in Fig. 2.

This paper is organized as follows. In the Theoretical section we describe the appropriate theory of heteronuclear dipolar ^{1}H–^{15}N and of quadrupolar ^{2}H T_1 relaxation in the presence of proton and deuteron transfer along a non-symmetric triple minimum potential following the stratagem of Latanowicz *et al.*[10] Then the results of the ^{15}N and ^{2}H T_1 relaxation time measurements on TTAA are reported and analyzed. Thus, rate constants of the proton and deuteron transfer are obtained in a wide temperature range. The data exhibit a non-Arrhenius behavior which is discussed in terms of a modified Bell tunneling model. This model allows us to address the question of how the formation of an intramolecular hydrogen bond influences the proton transfer barrier which is absent in the case of the thermal and IR-induced tautomerism of porphyrin which was studied by Moore *et al.*[17]

Theoretical section

Dipolar ^{15}N and ^{2}H relaxation theory of TTAA

The theory of nuclear spin relaxation in the presence of molecular motions, in the liquid or solid state is well established[18–20] and does not need to be repeated here. In this section, we focus on the effects of complex solid state proton transfers typical for a situation in TTAA according to Fig. 1b on the ^{15}N relaxation and of the corresponding deuteron relaxation on the solid state ^{2}H relaxation characteristics. For a more general formulation of the theory, we label the ^{15}N atoms a, c, d, f in Fig. 1b as spins *S* and the moving dipolar coupled protons b and e as spins *I*.

As the dipolar interaction represents an interaction between two spins *S* and *I*, it is characterized by the distance vector R^{SI}_r between the latter, as depicted in Fig. 2b for proton b. The subscript refers to the tautomeric states *r*, *s* = 1 to 4. When a proton jumps from state *r* to state *s*, the distance vector changes its length and its direction. The change of the direction is called the "jump angle" θ^{SI}_{rs}.

By contrast, the quadrupolar interaction of the deuteron spins *I* = b, e in the tautomeric state *r* can be described in terms of the single spin quadrupolar coupling tensor qcc^{I}_{r}. The largest tensor components of the deuterons b and e in TTAA are normally aligned parallel to the N–D distance vector. When the deuteron jumps, the tensors are rotated by the jump angles θ^{I}_{rs} as indicated for deuteron e in Fig. 2d.

The inverse longitudinal relaxation time of *S* in a single heteronuclear *IS* spin pair created by time-dependent fluctuations

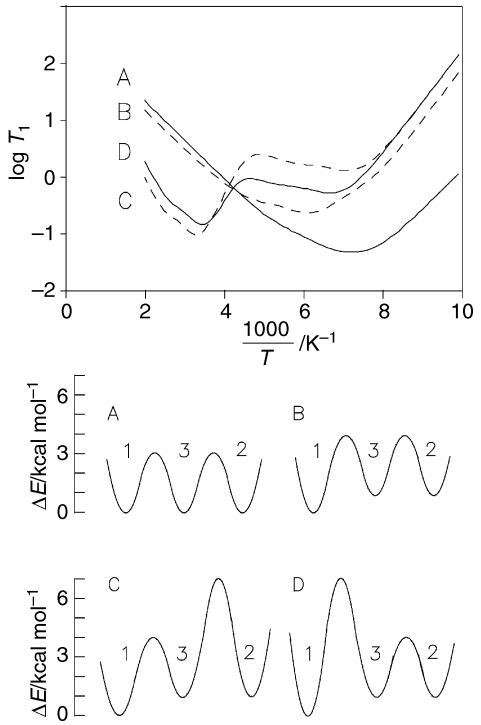

Fig. 3 Influence of a tautomeric interconversion 1 ⇄ 3 ⇄ 2 according to Fig. 1b on the calculated spin diffusion averaged ^{15}N relaxation times T_1 at 9.12 MHz plotted in a logarithmic scale as a function of the inverse temperature for different barriers indicated at the bottom for each reaction step. For the choice of the other parameters see text.

of the dipolar interaction is given by[1,18–20]

$$\frac{1}{T_{IS}} = (\mu_0/4\pi)^2 S(S+1) \times [\tfrac{1}{12}J_0(\omega_I - \omega_S) + \tfrac{3}{2}J_1(\omega_I) + \tfrac{3}{4}J_2(\omega_I + \omega_S)] \quad (1)$$

where I and S denote the spin of the two nuclei, ω_I and ω_S the associated Larmor frequencies, μ_0 the magnetic field constant, and $J_m(\omega)$ the Fourier intensities or spectral densities referring to the random fluctuations of the motion induced dipolar hamiltonian.

The spin–lattice relaxation of a nuclear spin I exhibiting an electric quadrupole moment is dominated by the motion-induced modulation of the electric field gradient at the nucleus. For the case $I = 1$ the resulting inverse spin lattice relaxation time is given by[8]

$$\frac{1}{T_{1I}} = \frac{9\pi^2}{8}(\mu_0/4\pi)^2[J_1(\omega_I) + J_2(2\omega_I)] \quad (2)$$

In this case the Fourier intensities $J_m(\omega)$ refer to the random fluctuations of the quadrupole interaction Hamiltonian.

As the spectral densities $J_m(\omega)$ depend on the fluctuations of the dipolar or the quadrupolar hamiltonian during the exchange processes, they depend in the case of a tautomeric exchange network according to Fig. 1 on the rate constants k_{rs} of the interconversion between states r and s and on the changes of the hamiltonians, *i.e.* in the case of a dipolar heteronuclear relaxation on the internuclear vectors R_r^{SI} and on the jump angles θ_{rs}^{SI} and in the case of a quadrupolar relaxation on the quadrupole coupling tensors qcc_r^I and the associated jump angle θ_{rs}^I.

For the case of only two interconverting states the spectral densities and ^{15}N relaxation times leading to a dipolar relaxation mechanism involving ^{15}N and ^{1}H were calculated by Hoelger *et al.*[15a] for a crystalline powder. The spectral densities $J_m(\omega_I)$ for the fluctuating part of the quadrupolar hamiltonian of jumping deuterons between two tautomeric state and the following deuteron T_1 relaxation times were calculated by Latanowicz and Reynhardt.[10e,f]

In the case of TTAA, in principle, exchange between up to four states has to be considered. However, as mentioned above, in practice the tautomeric state 4 is not populated within the margin of error.[14d] Therefore, we restrict the relaxation analysis to the case of three exchanging states. Both the isotropic dipolar ^{15}N–^{1}H relaxation as well as ^{2}H relaxation are considered. The appropriate expressions for the spectral densities $J_m(\omega)$ of dipolar and quadrupolar Hamiltonians are presented in the Appendix.

Once these expressions for the spectral densities in a given exchange model are known it is possible to express the relaxation rate of a spin S caused by a fluctuation of the heteronuclear dipolar interaction with spins I in terms of the equation

$$\frac{1}{T_{1S}} = (\mu_0/4\pi)^2 \frac{2}{15} S(S+1) \frac{N_I}{N_S^2} \times \sum_{S=1}^{N_S}\sum_{I=1}^{N_I}\{[X_2\, g(\tau_b) + X_3\, g(\tau_c)]\} \quad (3)$$

μ_0 is the magnetic field constant and S the spin of the observed nucleus, here 1/2 for ^{15}N.

In the case of TTAA, $N_S = 4$ represents the number of the ^{15}N spins S and $N_I = 2$ the number of dipolar coupled proton spins I. The functions $g(\tau)$ are given by

$$g(\tau_i) = \frac{\tau_i}{1 + (\omega_I - \omega_S)^2\tau_i^2} + \frac{3\tau_i}{1 + \omega_S^2\tau_i^2} + \frac{6\tau_i}{1 + (\omega_I + \omega_S)^2\tau_i^2} \quad (4)$$

In the case of quadrupole relaxation of spin I it follows that

$$\frac{1}{T_{1I}} = \frac{3\pi^2}{10}(\mu_0/4\pi)^2\left(1 + \frac{\eta^2}{3}\right)[X_2\, f(\tau_b) + X_3\, f(\tau_c)]. \quad (5)$$

where η is the asymmetry parameter and

$$f(\tau_i) = \frac{\tau}{1 + \omega_I^2\tau_i^2} + \frac{4\tau}{1 + 4\omega_I^2\tau_i^2}. \quad (6)$$

The correlation times τ_b, τ_c and the geometrical factors X_2 and X_3 are functions of the rate constants of the reaction network of Fig. 1b (excluding state 4), $\tau_i = f(k_{12}, k_{21}, k_{13}, k_{31}k_{23}, k_{32})$ and $X_i = f(k_{12}, k_{21}, k_{13}, k_{31}k_{23}, k_{32})$ explained in detail in Appendix 1.

Before the calculated relaxation times can be compared to experimental relaxation times it is necessary to take the effects of spin diffusion between nuclei exhibiting different relaxation times into account.[18] Spin diffusion strongly depends on the homonuclear dipolar interactions between the nuclei of interest. In contrast to the case of abundant ^{1}H spins, the dipolar interaction between ^{2}H spins is small so that we expect to measure two different relaxation times of the two deuterons b and e in TTAA. By contrast, even under MAS conditions spin diffusion between ^{15}N atoms in multiple-labeled compounds promoted *via* the heteronuclear dipolar interactions to ^{1}H is considerably fast.[21] In this case we expect a spin diffusion averaged ^{15}N relaxation time given by

$$\frac{1}{T_1} = \frac{1}{4}\left(\frac{1}{T_{1a}} + \frac{1}{T_{1c}} + \frac{1}{T_{1d}} + \frac{1}{T_{1f}}\right). \quad (7)$$

Only in the case of ^{15}N T_1 measurements at natural abundance—which is difficult in view of the small ^{15}N concentration—or at sufficiently low ^{15}N enrichment can the individual relaxation times be obtained.

Model calculations of dipolar ^{15}N relaxation theory of TTAA

In this section we present in Fig. 3 some numerical calculations of ^{15}N T_1 relaxation times as a function of the inverse

temperature for a model system chosen as close as possible to the situation in solid TTAA. The heteronuclear dipolar relaxation of the four inequivalent N atoms a to d arises from proton transfer steps between the states $1 \rightleftarrows 3 \rightleftarrows 2$ according to Figs. 1 and 2.

A computer program was written based on the theory presented above and in Appendix 1, where the individual relaxation times of each ^{15}N atoms a, c, d and e at 9.12 MHz and the spin diffusion averaged values are calculated, based on the hydrogen bond geometry of Fig. 2b. All short nitrogen atom distances r_{NH} to the nearest proton were set to 1.03 Å and the long distances $r_{N\cdots H}$ to 1.94 Å, and all dipolar jump angles to $\theta^d = 13.7°$. Arrhenius laws were assumed to describe the temperature dependence of each reaction step $1 \rightleftarrows 3$ and $3 \rightleftarrows 2$, where the pre-exponential factors $A_{13} = A_{31} = A_{23} = A_{32}$ were all set to the value of 2×10^{12} s^{-1}. Different cases A, B, C and D are considered involving different activation energies as indicated at the bottom of Fig. 3.

In case A we consider a symmetric energy reaction profile. A single ^{15}N T_1 minimum is obtained at low temperatures, as indicated at the top of Fig. 3. All relaxation times of the individual nitrogen atoms are the same. Let us now consider case B where state 1 is favoured over states 3 and 2. This implies that the nitrogen atom a exhibits a higher average proton density as compared to nitrogen d, and that nitrogen c exhibits a smaller average proton density than nitrogen f. This case is realized in TTAA as will be shown below. We assume that the barrier height of the step $3 \rightleftarrows 2$ was not changed as compared to case A. We obtain a single spin diffusion averaged ^{15}N T_1 minimum as in case A, but the relaxation times in the minimum become longer. Because of the symmetrized molecular structure the intrinsic relaxation times of the nitrogen atoms of a given hydrogen bridge are the same, but different for nitrogen atoms in different hydrogen bridges. The same is true for cases C and D where we did not change the thermodynamics of each proton transfer step but only the barrier heights. The two different barriers lead to two spin diffusion averaged ^{15}N T_1 minima, one at low temperature for the step with the smaller barrier, and another at high temperatures for the step involving the larger barrier. In case C the fast process corresponds to the interconversion $1 \rightleftarrows 3$ involving the jump of proton e between nitrogens d and f, whereas the slow process corresponds to the interconversion $3 \rightleftarrows 2$, where proton b jumps between nitrogen atoms a and c. Hence, it is clear that at low temperatures the intrinsic relaxation times of the nitrogen atoms d and f will be shorter than those of the nitrogen atoms a and c. In case D the situation is reversed. If we compare the T_1 values in the low-temperature minimum we observe that in case D these values are shorter as compared to case C because the relaxation active proton transfer step is energetically more symmetric. The same argument leads to shorter T_1 values in the high temperature minium for case C.

As mentioned above, longitudinal quadrupolar ^2H relaxation is much shorter than heteronuclear dipolar ^{15}N–^1H relaxation, and ^2H spin diffusion is normally not relevant. Therefore, it follows that the two different deuterons b and e will exhibit different relaxation times. In case C, deuteron e will relax faster than deuteron b, whereas in case D the contrary will be realized. In conclusion, it is desirable to measure the intrinsic ^{15}N relaxation times in order to elucidate the relative barrier heights of the two transfer steps.

Experimental section

Polycrystalline TTAA–$^{15}N_4$ (tetramethyldibenzotetraaza[14]annulene-N_4) was prepared as described previously.[14] For the ^2H NMR measurements the compound was deuterated in the inner proton sites by recrystallizing it three times from CH_3OD 98%, commercially available from Deutero GmbH. The measurements of the ^2H T_1 relaxation times for these deuterons were performed on a 7 T Bruker CXP300 spectrometer operating at a Larmor frequency of 46 MHz equipped with a home built low temperature ^2H probe. The measurements were carried out employing a saturation recovery pulse sequence follow by a quadrupolar echo sequence and recording of the echo. The saturation part involved a string of 90° pulses with non-equal spacing to avoid any undesired echo formations. The sequence was followed by Fourier transformation of the echo, allowing the measurement of separate spectral lines from deuterons as well as the evaluation of T_1 for individual lines in the spectrum. The ^2H T_1 measurements were performed in the temperature range from 90 to 300 K.

The ^{15}N T_1 relaxation times of TTAA-$^{15}N_4$ were measured between 128 and 366 K using a Bruker CXP 100 NMR spectrometer at 2.1 T, corresponding to a Larmor frequency of 9.12 MHz for ^{15}N under CPMAS conditions. Some experiments were performed at 30.41 MHz at natural ^{15}N abundance. The line positions of the TTAA are highly sensitive to the temperature.[14] The ^{15}N T_1 measurements were recorded using the usual pulse sequence described by Torchia where no proton decoupling is applied during the equilibration period of time.[22] In order to suppress artifacts arising from a distorted base line and from acoustic ringing the scheme of Du Bois Murphy was employed.[23] The 90° pulse width was 3.6 μs for ^2H and 6 μs for ^{15}N. The spinning frequency of 2 kHz was sufficient to obtain spectra free of rotational sidebands. For each ^2H-spectrum, between 500 and 1000 scans were accumulated; for ^{15}N between 24–200 scans were accumulated.

Results

^{15}N CPMAS NMR spectroscopy of TTAA

The 9.12 MHz ^{15}N CPMAS NMR spectra of polycrystalline TTAA-$^{15}N_4$ have been described in ref. 14. The spectra taken between 86 and 405 K are depicted in Fig. 4. As described previously,[14] four lines a to d are observed with strong temperature-dependent line separations $\delta_{ac} = \delta_a - \delta_c$ and $\delta_{df} =$

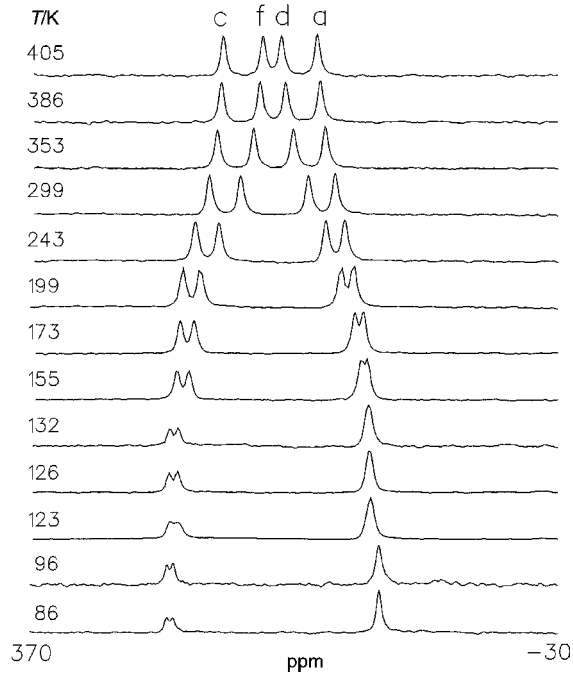

Fig. 4 9.12 MHz ^{15}N CPMAS NMR spectra of 95% ^{15}N enriched TTAA at 9.12 MHz as a function of temperature; 6–10 ms cross-polarization time, 7 kHz spectral width, 2.7 s repetition time, 100 scans on average, 2–2.8 kHz rotation frequency, single nitrogen gas supply for sample bearing and driving. Adapted from ref. 14(*d*).

δ_d–δ_f. ^{15}N spin-diffusion measurements showed that this dependence is due to the fact that each TTAA molecule contains four chemically inequivalent nitrogen atoms a, c, d and f characterized by different temperature-dependent average proton densities.[14] Finally, we note that deuteration of the inner proton sites does not affect at all the line positions indicating absence of equilibrium isotope effects on the proton tautomerism of TTAA.

Thermodynamics of proton transfer in TTAA

The variation of the splittings δ_{mn} between the lines mn = ac and df as a function of temperature were evaluated in a quantitative way on the basis of the reaction network shown in Fig. 1b as follows. Due to solid-state effects the gas-phase degeneracies between the tautomeric states 1 and 2 as well as between 3 and 4 are lifted. The single reaction steps in Fig. 1b are characterized by the equilibrium constants[14d]

$$K_{rs} = x_s/x_r = \exp(-\Delta H_{rs}/RT + \Delta S_{rs}/R) \quad (8)$$

where x_{rs} are the mole fractions of the tautomeric states r and s, T the absolute temperature and R the gas constant. ΔS_{rs} and ΔH_{rs} are the molar entropy differences and molar enthalpy differences of the reaction step r to s. The equilibrium constants can be obtaind as follows. From the temperature dependent line separations δ_{mn} the average proton density ratios can be calculated[14] from

$$K_{mn} = (1 - \delta_{mn}/\Delta_{mn})/(1 + \delta_{mn}/\Delta_{mn}), \quad mn = \text{ac, df}, \quad (9)$$

where Δ_{mn} is the intrinsic chemical shift difference of the hydrogen-bonded atoms m and n in N_m–H···N_n obtained at low temperature, where $K_{mn} \approx 0$. The proton density ratios are given by

$$K_{ac} = (x_2 + x_4)/(x_1 + x_3) = (K_{12} + K_{14})/(1 + K_{13}) \quad (10)$$

and

$$K_{df} = (x_2 + x_3)/(x_1 + x_4) = (K_{12} + K_{13})/(1 + K_{14}) \quad (11)$$

where

$$K_{12} = K_{13}K_{32} = K_{14}K_{42}. \quad (12)$$

The line positions were analyzed as follows. First, the values of K_{ac} and K_{df} were calculated using eqn. (9) and the low temperature splittings Δ_{ac} = 143.4 ppm and Δ_{df} = 140.5 ppm. Then, a simultaneous non-linear least-squares fit of the experimental ln K_{ac} and ln K_{df} values *vs.* $1/T$ was performed, which allowed the determination of the parameters $\Delta H_{13} = \Delta E_{13}$, ΔS_{13}, $\Delta H_{32} = \Delta E_{32}$, ΔS_{32} and $\Delta H_{14} = \Delta E_{14}$, ΔS_{14}. The result of this fit is shown in Fig. 5 and the parameters obtained are assembled in Table 1. The temperature dependence of the important reactions $1 \rightleftarrows 3 \rightleftarrows 2$ can also be expressed as

$$K_{13} = k_{13}/k_{31} = 1.21 \exp(-560/T),$$
$$K_{32} = k_{32}/k_{32} = 1.66 \exp(-34T),$$
$$K_{14} = k_{14}/k_{41} \approx 0, \quad 100 \text{ K} < T < 400 \text{ K}. \quad (13)$$

This result can be interpreted in terms of the temperature dependent mole fractions x_r of the various forms, depicted in Fig. 6. The most stable form is the *trans* form 1 in Fig. 1b; due to solid-state effects the second *trans* form 2 has a higher energy than 1. The energy of the *cis* form 3 has approximately

Table 1 Equilibrium parameters of the TTAA tautomerism according to ref. 14(*d*)[a]

$\Delta H_{13} = \Delta E_{13}$	ΔS_{13}	$\Delta H_{32} = \Delta E_{32}$	ΔS_{32}	$\Delta H_{14} = \Delta E_{14}$	ΔS_{14}
4.65	2.25	0.29	4.22	$\gg 0$	—

[a] Energies in kJ mol^{-1}, entropies in J K^{-1} mol^{-1}.

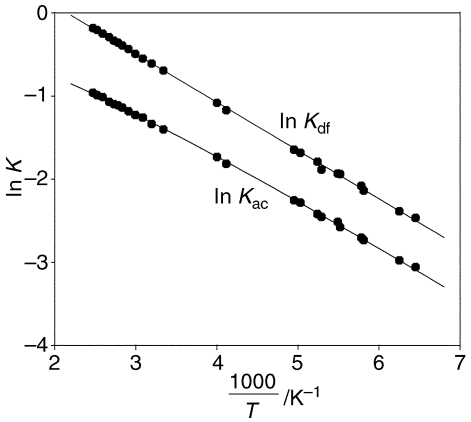

Fig. 5 Logarithmic simultaneous non-linear least-squares fit of the proton density ratios K_{ac} and K_{df} in the hydrogen bonds abc and def according to eqns. (14) and (15) as a function of the inverse temperature from which the equilibrium constants K_{13}, $K_{32} > 0$ and $K_{32} \approx 0$ are determined.

the same energy as form 2; the *cis*-tautomer 4 is not populated to an observable extent. This situation corresponds to the relative locations of the energy minima at the bottom of Fig. 3, where, however, a distinction between cases C and D is not yet possible.

Hydrogen bond structure of crystalline TTAA

For the interpretation of the ^{15}N relaxation data in the forthcoming section we needed information on the proton locations in the hydrogen bonds of TTAA. Since X-ray crystallography can not provide these locations accurately[24]—a task which is particularly difficult in the case of TTAA because of the proton tautomerism—and since no neutron structure was available we used the hydrogen bond structure depicted in Fig. 2d which was derived as follows.

We assumed that hydrogen atoms are located in the molecular plane, and that the short NH distances r_{NH} and the long NH distances $r_{N\cdots H}$ are the same for all hydrogen bonds in each of the four tautomers. First we set r_{NH} = 1.03 Å which is within the margin of error identical with the value of 1.04 Å obtained by dipolar relaxometry and dipolar ND-coupling for the related DTAA molecule.[15a,25] The slightly smaller value was later justified by least squares fit of the relaxation data. Knowing the short N–H distance, we made use of the well-known correlation between r_{NH} and $r_{H\cdots N}$ of NHN–H bonds established by neutron diffraction,[26] NMR and theoretical calculations[27a]

$$r_{H\cdots N} = r_0 - l \ln[1 - \exp\{-(r_{NH} - r_0)/b\}], \quad (14)$$

where r_0 = 0.99 Å and b = 0.404 Å.[27a] Using eqn. (14) we obtained a long N···H distance of 1.94 Å. Taking into

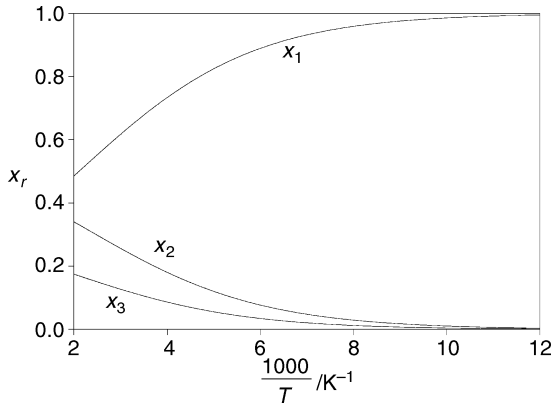

Fig. 6 Calculated mole fractions x_r of the tautomers 1, 2 and 3 of polycrystalline TTAA as a function of the inverse temperature.

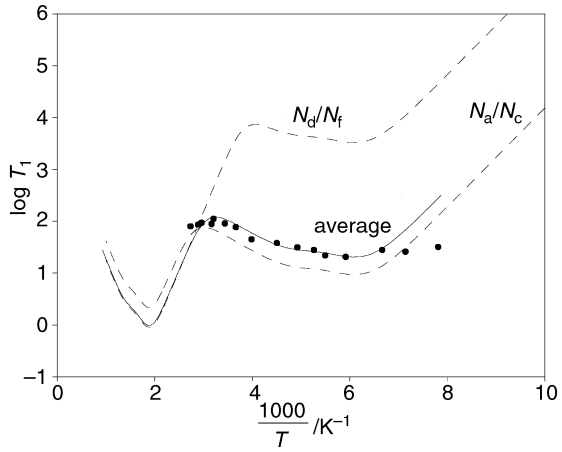

Fig. 7 Temperature dependence of the spin diffusion averaged ^{15}N T_1 relaxation time of polycrystalline TTAA at 9.12 MHz. The solid line was calculated according to eqn. (3) using the fixed ratios $A_{31}/A_{13} = 1.31$ and $A_{32}/A_{23} = 1.66$ derived in eqn. (17) and parameter fit of $A_{13} = 1.6 \times 10^{12}$ s^{-1}, $E_{23} = 14$ kJ mol^{-1}, $E_{31} = 41$ kJ mol^{-1}, and the NH bond length 1.04 Å (see text). The dashed lines correspond to the intrinsic relaxation times of the nitrogen pairs Na/Nb and Nc/Nd. The T_1 values of the two nitrogen atoms in each pair are identical.

account the crystallographic distance of $r_{NN} = 2.675$ Å between the two nitrogen atoms of a given hydrogen bond and of $r_{NN'} = 2.699$ Å between closest nitrogen neighbors in different hydrogen bonds,[16] we thus derived the proton positions of Fig. 2d. We obtain pronounced non-linear hydrogen bonds exhibiting a hydrogen bond angle of $\alpha = 134°$. Now, it follows that during a proton jump the distance to a given nitrogen atom changes from 1.03 to 1.94 Å, involving a dipolar jump angle of $\theta^d = 13.7°$. For the quadrupolar jump angle it follows that $\theta^d = 104°$.

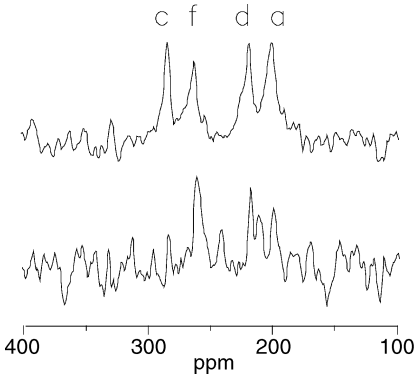

Fig. 8 ^{15}N CPMAS inversion recovery spectra of TTAA at natural ^{15}N abundance for delay times of 1 ms and 20 s.

^{15}N T_1 measurements and analysis

^{15}N T_1 experiments at 9.12 MHz were performed on TTAA–$^{15}N_4$ in the temperature range between 128 and 366 K. All signals a, c, d and f of Fig. 4 exhibited a common exponential longitudinal relaxation described by a single relaxation time averaged by spin diffusion. The values obtained are assembled in Table 2 and plotted in Fig. 7 in a logarithmic scale as a function of the inverse temperature. T_1 decreases slightly when temperature is decreased, reaching a minimum near 170 K. A calculation of the slope of ln T_1 *vs.* $1/T$ leads to a suspiciously small activation energy in a large temperature range less than 14 kJ mol^{-1} found usually only in the neighborhood of a T_1 minimum or for extremely fast proton transfers at low temperature. For a long time we were puzzled by this result, until we realized that this feature can easily be explained in terms of cases C and D in Fig. 3.

In order to distinguish between both cases we tried to perform ^{15}N T_1 experiments on TTAA at natural ^{15}N abundance. In this case practically only singly ^{15}N labeled TTAA molecules are observed, where the label is located with equal probability in the four atomic sites a, c, d and f. A natural abundance ^{15}N T_1 experiment should then lead to the individual non-spin diffusion averaged relaxation times. Unfortunately, because of sensitivity problems our attempts to measure these data at 9.12 MHz were not successful. In addition, a corresponding experiment at 30.41 MHz was also difficult. Nevertheless, an outcome of such an experiment is depicted in Fig. 8, where two spectra are shown, one at a relaxation delay of 1 ms and the other of 20 s. Although the signal to noise ratio is poor, we have a good indication that the outer lines arising from nitrogen atoms a and c exhibit the shorter relaxation times. As already discussed in the Theoretical section, this qualitative result indicates that case D is realized, otherwise the inner nitrogen lines would have the shorter relaxation time. The analysis in terms of case D leads in Fig. 7 to the dashed lines for the individual relaxation times of nitrogen atoms a, c and of d, e, and to the solid line corresponding to the spin diffusion averaged relaxation times calculated from the individual times according to eqn. (3). An idea to obtain the individual ^{15}N T_1 times for each nitrogen with a better signal to noise ratio was to measure a 10% ^{15}N-labeled compound mixed 1 : 1 with unlabeled TTAA, but it turned out, that even in this sample the spin diffusion is still present, leading to an average T_1 value for all signals. Fig. 9a and 9b show the T_1 and spin diffusion measurements for both samples at 300 MHz. It is obvious, that spin diffusion is slower in the case of $^{14}N/^{15}N$ TTAA than for fully labeled TTAA, but still much faster than the spin lattice relaxation time. The parameters used to calculate the lines in Fig. 7 are assembled in Table 3 and will be discussed in the following.

As in the model calculations of Fig. 3, we assumed Arrhenius laws to describe the temperature dependence of the rate constants, *i.e.* $k_{13} = A_{13}\exp(-E_{a13}/RT)$ and $k_{32} = A_{32}\exp(-E_{a23}/RT)$. The equilibrium constants of each reaction step were already given in eqn. (13). Furthermore, we set $A_{13} = A_{32}$ and varied in the non-linear least squares fitting

Table 2 ^{15}N T_1 relaxation times for TTAA at 9.12 MHz in the solid state and proton transfer rate constants of the TTAA tautomerism in the solid state (* Arrhenius behaviour assumed)

T/K	T_1/s	k^H_{23}/s^{-1}	k^H_{31}/s^{-1}	T/K	T_1/s	k^H_{23}/s^{-1}	k^H_{31}/s^{-1}
366	80	1.36×10^{10}	5.44×10^{6}	222	38	1.43×10^{9}	746.6*
346	86	1.29×10^{10}	2.57×10^{6}	203	31.5	8.03×10^{8}	84.50*
338	94	1.23×10^{10}	1.71×10^{6}	190	28	5.16×10^{8}	16.03*
316	89	9.97×10^{9}	7.02×10^{5}	182	22	3.66×10^{8}	5.94*
312	112	9.26×10^{9}	5.01×10^{5}	169	20	2.12×10^{8}	0.45*
291	91	4.44×10^{9}	2.18×10^{5}*	150	28	8.03×10^{7}	0.03*
273	77	3.61×10^{9}	4.29×10^{4}*	140	26	4.36×10^{7}	0.0032*
251	45	2.14×10^{9}	1.03×10^{4}*	128	32	4.04×10^{7}	0.000 24*

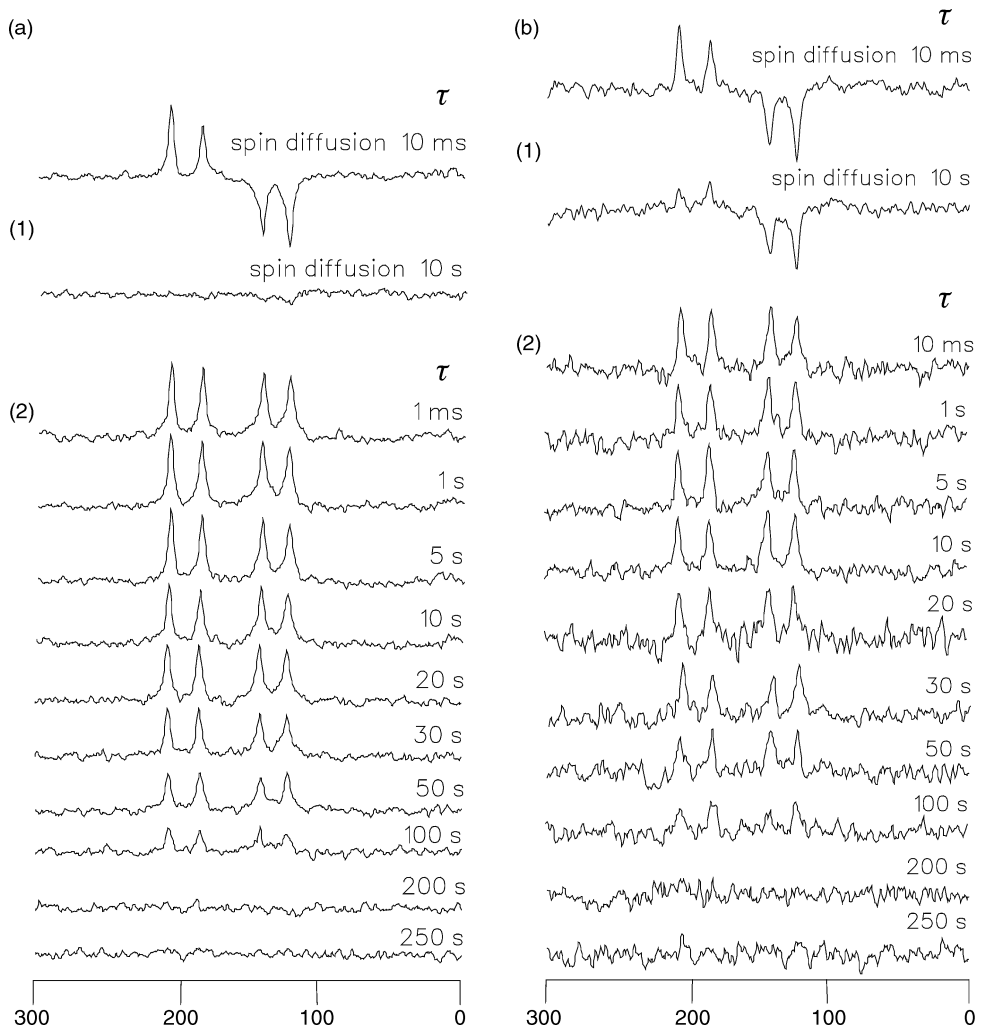

Fig. 9 (a) Spin diffusion (1) and ^{15}N T_1 measurement (2) for fully ^{15}N-labelled TTAA after different delay times τ. (b) Spin diffusion (1) and ^{15}N T_1 measurement (2) for 10% ^{15}N-labeled TTAA after different delay times τ.

routine only E_{a13} and E_{a32}. The geometrical parameters were those described in the previous section.

By adapting the short distance to 1.03 Å, we obtain the solid line in Fig. 7, which compares very well with the experimental data points. At high temperatures the values are both determined by k_{13} and k_{32}, leading to the almost horizontal curve. By contast, at low temperatures the relaxation is prominantly determined by the values of k_{32}. We note a substantial deviation between the calculated and experimental T_1 values in this temperature region which we ascribe to tunneling.

In order to obtain tunneling model independent rate constants k_{32} at each temperature we wrote a computer program which allowed us to convert each ^{15}N T_1 value into a value of k_{32}. As the relaxation data are not influenced much at low temperature by k_{13} we kept the assumption of an Arrhenius type dependence of this quantity. All rate constants obtained are included in Table 2. Note, however, that the low-temperature values of k_{13} are not corrected for tunneling.

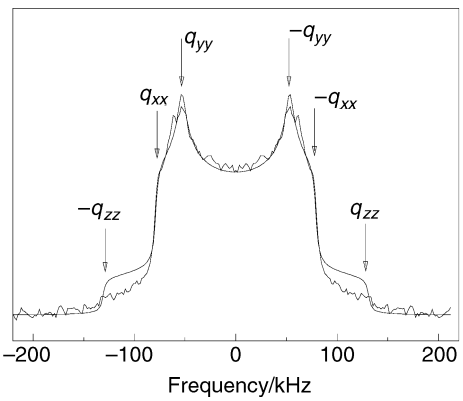

Fig. 10 Superposed experimental and simulated ^2H-NMR spectrum of TTAA-d_2 at 100 K. For further explanation see text.

^2H NMR spectroscopy of TTAA

Fig. 10 shows the ^2H NMR spectrum of the TTAA recorded at 100 K. While there are two deuterons b and e present in the TTAA, only a single signal is visible, exhibiting the typical Pake pattern. This observation indicates that the two deu-

Table 3 Parameters of the 9.12 MHz ^{15}N T_1 analysis of TTAA[a]

r_{NH}/Å	r_{NN}/Å	$r_{NN'}$/Å	$r_{N\cdots H}$/Å	α/°	θ^d/°	E_{a23}/kJ mol^{-1}	A_{23}/s^{-1}	E_{a31}/k J mol^{-1}	A_{31}/s^{-1}
1.03	2.675	2.699	1.94	134	13.7	14.0	0.8×10^{12}	41.0	0.8×10^{12}

[a] r_{NH}: short NH distances in all tautomers, extrapolated from dipolar NMR data of DTTA according to refs. 15(*a*) and 25. r_{NN} and $r_{NN'}$: N···N distances within and between the two hydrogen bridges according to the X-ray structure of TTAA (see Fig. 2b).[16] $r_{N\cdots H}$: long NH distances calculated using the hydrogen bond correlation (eqn. (18)) from r_{NH} and r_{NN}. α: hydrogen bond angle calculated from r_{NH}, $r_{N\cdots H}$ and r_{NN}. θ^d dipolar proton jump angle (Fig. 2b). The other parameters were obtained by non-linear least squares fit to the experimental data taking into account eqn. (11), leading to the solid line in Fig. 7.

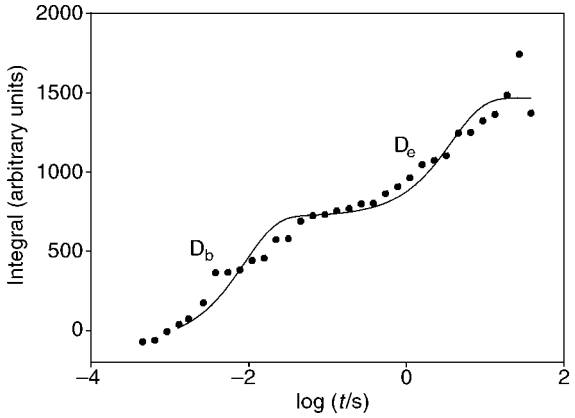

Fig. 11 Results of a 46 MHz deuteron spin–lattice relaxation time experiment performed on TTAA-d_2 at 298 K. From a bi-exponential fitting procedure the T_1 values of 31 ms and 5.6 s were obtained for deuterons b and e.

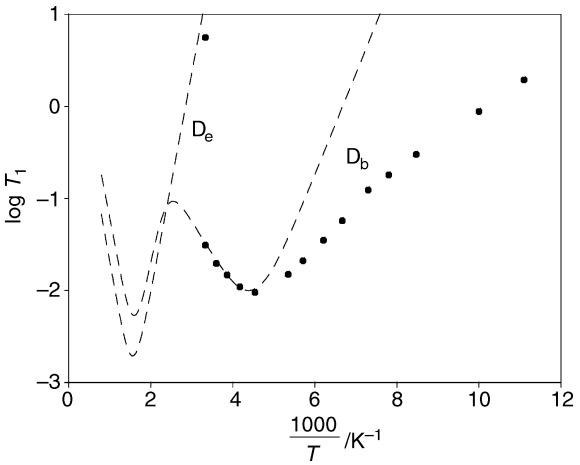

Fig. 12 T_1 values of deuterons b and e in TTAA plotted in a logarithmic scale as a function of the inverse temperature. The fit parameters are listed in Tables 5 and 6.

Table 4 ^{2}H T_1 relaxation times and deuteron transfer rate constants in solid TTAA

T/K	T_{1b}/s	T_{1e}/s	k^D_{32}/s^{-1} [a]	k^D_{13}/s^{-1} [a]
300	0.031	5.6	3×10^9	7.9×10^8
278	0.0196	—	1.7×10^9	4.7×10^8
259	0.0147	—	1.1×10^9	2.8×10^8
240	0.0109	—	6.3×10^8	1.3×10^8
220	0.0095	—	4.3×10^8	5.7×10^7
187	0.0149	—	1.3×10^8	2.0×10^7
175	0.021	—	8.8×10^7	1.2×10^7
161	0.035	—	4.9×10^7	7.0×10^6
150	0.057	—	3.3×10^7	4.2×10^6
137	0.0123	—	1.8×10^7	1.7×10^6
128	0.0180	—	1.2×10^7	1.1×10^6
118	0.3	—	8.3×10^6	6.6×10^5
100	0.88	—	3.8×10^6	2.3×10^5
90	1.94	—	1.7×10^6	1.1×10^5

[a] Either k_{32} or k_{13}.

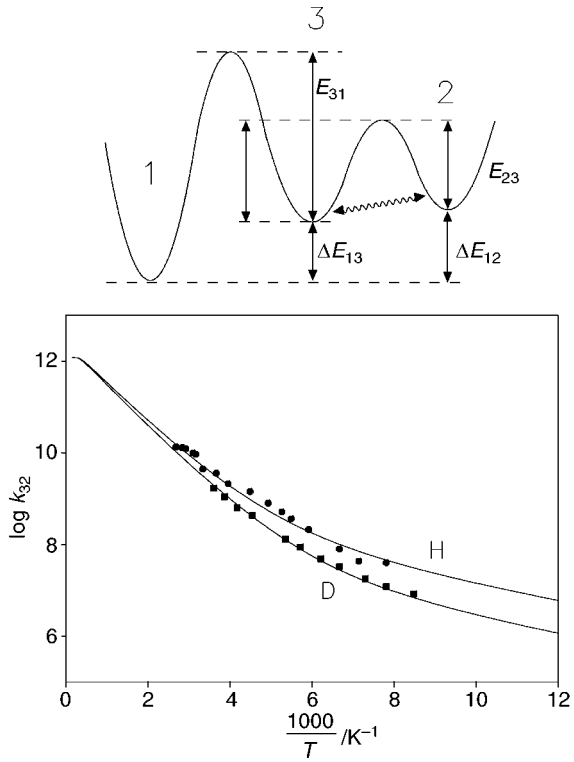

Fig. 13 Arrhenius diagram of the relaxation active proton and deuteron transfer step 3 ⇄ 2 of the solid state tautomerism of TTAA. The solid lines were calculated using a modified Bell tunneling model as described in the text.

terons exhibit similar quadrupole coupling tensors. A line shape analysis was performed and the calculated spectrum is included in Fig. 10, leading to the parameters $q_{xx} = -78$ kHz, $q_{yy} = -53$ kHz, $q_{zz} = 131$ kHz. The results can also be expressed in terms of the quadrupole coupling constant $qcc = 4/3q_{zz} = 175$ kHz for both deuterons, and the asymmetry parameter $\eta = (q_{yy} - q_{xx})/q_{zz} = 0.19$. q_{zz} is assumed to coincide with the directions of the N–D bonds as indicated in Fig. 2d.

When the deuterons jump their quadrupole interaction is modulated which could lead to line shape changes. For TTAA we were, however, not able to observe any changes in lineshape in the measured temperature range.

Longitudinal ^{2}H relaxation analysis

In Fig. 11 we have depicted the results of a room temperature ^{2}H saturation T_1 relaxation experiment on doubly deuterated TTAA. We observe a bi-exponential dependence of the integrated magnetization M as a function of time t which can be described in terms of the equation

$$M = [M_{\infty b}(1 - \exp(-t/T_{1b})) + M_{\infty e}(1 - \exp(-t/T_{1e}))], \quad (15)$$

where $M_{\infty b} = M_{\infty e}$ represents the integrated intensities of deuterons b and e at infinite times between saturation pulses and T_{1b} and T_{1e} the corresponding relaxation times. As the two relaxation times were very different we use log t as the abscissa in Fig. 11. We assign the longer relaxation time of 5.6 s to deuteron e and the short time of 31 ms to deuteron b.

Table 5 Parameters of the 46 MHz ^{2}H T_1 analysis of TTAA

q_{zz}/kHz	η_{zz}	θ^q/°	E_{a23}/kJ mol^{-1}	A_{23}/s^{-1}	E_{a31}/kJ mol^{-1}	A_{31}/s^{-1}
175[a]	0.19[a]	104.2[b]	17.3	1.2×10^{12}	42	1.2×10^{12}

[a] Line shape analysis of Fig. 10. [b] θ^q: quadrupolar jump angle according to Fig. 2d. The other parameters were determined as described in the text, leading to the dashed lines in Fig. 12.

Further relaxation experiments were performed at lower temperatures, however, only the short time T_{1b} was measured.

The results of the deuterium NMR T_1 measurements are assembled in Table 4 and are plotted in Fig. 12 in a logarithmic way as a function of $1/T$. A minimum of T_{1b} is observed around 220 K. Thus, at this temperature the rate constant k_{23} of the jump of deuteron b which modulates its quadrupole interaction is given approximately by the ^{2}H Larmor frequency of 46 MHz. The calculated curve predicts a second minimum around 500 K which is experimentally not accessible. The activation energies and pre-exponential factors in Table 5 were fitted to the data in the temperature region between 300 and 220 K, taking into account eqn. (5), and keeping the quadrupolar jump angles constant. Note, that we performed a simultaneous data fit both of T_{1b} and T_{1e} which reproduces well the high temperature data. At low temperatures, we observe again a deviation from the calculated data which indicates again that the apparent activation energy E_{a23} decreases due to tunneling.

As in the nitrogen case, in the last step of the analysis we converted the relaxation times into rate constants k_{32} of the transfer of deuteron b. The results obtained are included in Table 4. Again, we assumed that at low temperatures the neglect of the tunnel contribution for k_{13} does not affect substantially the results. Finally, we plot in Fig. 13 the rate constants k_{32} in a logarithmic way as a function of the inverse temperature. A pronounced non-Arrhenius behavior with a concave curvature is observed both for the proton and the deuteron transfer which is indicative of tunneling.

Discussion

We have reported in the previous sections a study of the stepwise proton transfer in TTAA. Both information about the thermodynamics and the kinetics of the proton transfer was obtained. We note that at the highest temperature where the rate constant could be measured, values are about 10^{10} s^{-1} which corresponds to 100 ps. This is surely a significant progress as NMR is usually regarded as a slow kinetic tool.

Let us first discuss the thermodynamic results. The ^{15}N CPMAS spectra showed four inequivalent nitrogen atoms which were consistent only with a stepwise reaction network of Fig. 1b. In the absence of intermolecular interactions, states 1 and 2 as well as states 3 and 4 would be pairwise equivalent, leading to the same average proton densities of 0.5 on all nitrogen atoms. However, in the solid state these degeneracies are lifted by intermolecular interactions, and the two hydrogen bonds in solid TTAA become non-equivalent, *i.e.* one nitrogen atom of a hydrogen bond exhibits a larger and the other a smaller average proton density. The nitrogen atom pair a and c is the one exhibiting the larger difference in proton densities. Unfortunately, we were not able to localize the two hydrogen bridges in the unit cell. By a careful chemical shift analysis we showed that state 4 is not formed in the temperature range covered, that the reaction step $1 \rightleftarrows 3$ is quite asymmetric and that the reaction step $3 \rightleftarrows 2$ is quasi-symmetric with respect to energy. Thus, we could restrict our relaxation analyses to the reaction sequence $1 \rightleftarrows 3 \rightleftarrows 2$. An appropriate theory both for ^{15}N relaxation from which the dynamics of the proton transfer was derived and of ^{2}H relaxation was formulated in order to convert the longitudinal relaxation times into rate constants. In Fig. 3 we discussed for this sequence four different reaction mechanisms where only cases C and D were in agreement with the thermodynamic results. By ^{15}N relaxation we were able to distinguish between both possibilities. In case C the first asymmetric reaction step where proton e is transfered exhibits a smaller barrier than the second step where proton b is transferred. At low temperatures, proton e relaxes then its nitrogen neighbors d and f *via* step $1 \rightleftarrows 3$ more efficiently than proton b and its neighbors a and c in step $3 \rightleftarrows 2$. On the other hand, in case D proton b moves fast in step $3 \rightleftarrows 2$, and the relaxation of nitrogen atoms a and c is more efficient than the relaxation of nitrogen atoms d and f. Unfortunately, ^{1}H mediated spin diffusion averages out these relaxation differences in the fully ^{15}N labeled TTAA sample on which most experiments were performed because of the very good signal to noise ratio the isotopic enrichment provides. Nevertheless, one experiment was performed on TTAA at natural ^{15}N abundance where spin diffusion is not operative. This experiment whose results were reported in Fig. 8 provided good evidence that the outer lines arising from nitrogen atoms a and c relax faster than the inner lines arising from nitrogen atoms d and f. Thus, evidence was provided that case D in Fig. 3 is realized.

By contrast, in the case of ^{2}H relaxation two different relaxation times were observed, where the longer time could now be assigned to deuteron e and the shorter time to deuteron b. This analysis allowed us now to convert the relaxation data into rate constants k_{32}^{H} and k_{32}^{D} of the second reaction step $2 \rightleftarrows 3$ in Fig. 1b, without assuming a particular model for the dependence of these rate constants on temperature. By contrast, the rate constants k_{13}^{H} and k_{13}^{D} could be obtained from the relaxation data only assuming the validity of the Arrhenius law.

The values of k_{32}^{H} and k_{32}^{D} are plotted in the Arrhenius diagram of Fig. 12 in a logarithmic way as a function of the inverse temperature. We observe strong deviations from an Arrhenius behavior in the sense that the rate constants at lower temperatures are larger than expected leading to a concave curvature of the Arrhenius curves. This behavior is typical for tunneling pathways at low temperatures, as already pointed out by Bell.[28] It also generally leads to anomalous kinetic H/D-isotope effects. In the past we have observed such phenomena in a number of cases involving single or double[11] intramolecular proton transfers[11,15a,15c] or intermolecular triple proton transfers.[13] Tunneling phenomena have also

Table 6 Parameter of the modified Bell model of the tautomerism of porphyrin, the porphyrin anion, porphycene and TTAA[a]

	k^H (250 K)	k^H/k^D (250 K)	E_d	E_m	$E_d + E_m$	log A	$2a$	m_H	m_D	Δm	$\Delta\varepsilon$
Porphyrin[11e]	820	24	28.7	22.7	51.4	12.6	0.68	1	2	1.5	1.5
Porphyrin anion[11e]	20 760	106	34.3	10.0	44.3	12.6	0.78	1	2	1.5	1.5
Porphycene stepwise single H transfer[15c]	1.2×10^7	—	25.9	5.9	31.8	12.6	0.64	1	2	1.5	—
Porphycene correlated HH transfer[15c]	1.2×10^7	—	25.9	5.9	31.8	12.6	0.56	2	4	1.5	—
DTAA[15a]	2.7×10^5	—	—	—	33.5	12.1	—	—	—	—	—
TTAA	2.14×10^9	3.3	14.2	2.9	17.1	12.4	0.50	1	2	3	3

[a] Barrier height E_d and minimum energy for tunneling E_m in kJ mol^{-1}, additional barrier energy for the deuteron motion $\Delta\varepsilon$ in kJ mol^{-1}, barrier width $2a$ in Å, frequency factor A in s^{-1}. Tunneling masses $m_{eff}^{L} = m_L + \Delta m$, L = H, D.

been observed in other systems such as the tautomerism of benzoic acid dimers in the solid state.[1–10] Whereas the purely physical approach consists of formulating an appropriate relaxation theory in the presence of proton and deuteron tunneling we converted our relaxtion data without assuming a particular tunneling model into rate constants, as mentioned above. This procedure leaves room in the future for more sophisticated tunneling models which will then not need to include the theory of relaxation, but only an appropriate theory of rate processes.

Here, we will restrict ourselves to rationalize our data in terms of a simple one-dimensional modified Bell tunneling model as indicated in Fig. 13. This model has been described in detail.[11] The model contains the following adjustable parameters: (i) E_m represents the minimum energy for tunneling to occur; (ii) E_d^H is the barrier height for the proton transfer at the energy E_m; (iii) the D transfer involves the additional barrier energy $\Delta_\varepsilon^D = E_d^D - E_d^H$; (iv) $2a$ is the barrier width of the H transfer in Å at the energy E_m; (v) a single frequency factor A in s^{-1} is used for all isotopic reactions, *i.e.* a possible mass dependence Bell $A^H : A^D \approx 1^{-1/2} : 2^{-1/2}$ is assumed to be negligible within the margin of error; (vi) the tunneling masses are assumed to be given by $m_{eff}^L = m^L + \Delta m$, with the fixed values $m^H = 1$, $m^D = 2$. Δm takes into account the possibility of small heavy atom displacements during the tunnel process.

The solid lines in Fig. 13 were calculated in terms of this model *via* a simultaneous non-linear least squares fit of both Arrhenius curves, by freely varying all parameters. The agreement between the experimental and calculated data is satisfactory. The resulting parameter values are listed in Table 6. Because of the unrealistic simplicity of the one-dimensional tunneling model one should not attribute too much physical significance to these parameters although they seem reasonable. The barrier width is of the order expected for the hydrogen bonds of TTAA. The tunneling masses had to be substantially increased as compared to the simple proton or deuteron masses in order to reproduce the experimental kinetic H/D isotope effects. The barrier height is the most realistic parameter as it comes essentially from the high temperature slopes of the Arrhenius curves. In this region, we find a somewhat higher effective barrier for the deuteron transfer indicating as usual a loss of zero point energy in the transition state as predicted by Bell.[28]

In Table 6 the barrier parameters are compared to those of related intramolecular proton transfers studied previously in our group. The most interesting observation is the very small barrier of proton transfer in TTAA. This barrier is much smaller than for the related DTAA molecule studied in ref. 15(*a*), where we had offered already a qualitative explanation for this difference. In the case of DTAA the two hydrogen bonds are thermodynamically coupled in the sense that proton transfer in one bond favors proton transfer in the other. This means that in DTAA only the diagonal tautomers 1 and 2 are populated to an observable extent as indicated in Fig. 1a, and that the vicinal tautomers 3 and 4 represent high-energy intermediates of the stepwise proton transfer. This coupling occurs because the two H-chelate units of DTTA are probably located in a single molecular plane, in contrast to TTAA where this arrangement is not possible because of steric interactions between the methyl groups and the aromatic hydrogen atoms. This difference has been discussed already a long time ago,[14,15a] supported by the observation of a red color of DTAA and yellow color of TTAA. In TTAA, the *cis*-tautomers are, therefore, drastically reduced in energy as compared to DTAA, leading also to a smaller barrier for the proton transfer processes.

The smaller proton transfer barrier in TTAA as compared to the stepwise proton transfer in porphycene[15c] is less easily explained, in view of the fact that this molecule contains stronger hydrogen bonds than TTAA, which is supported by the finding of an N–H distance of 1.1 Å as compared to the 1.03 Å in TTAA. The faster process in TTAA leads already to a ^{15}N T_1 minimum at 170 K as compared to a ^{15}N T_1 minimum for porphycene at 280 K and 9.12 MHz caused by the moving proton. In ref. 15(*c*) we were, however, not able to distinguish whether the double proton transfer observed in porphycene is stepwise or concerted, which leads to the two entries in Table 6. As generally concerted quasi-degenerate double proton transfers imply the weakening or breaking of two hydrogen-heavy atom bonds instead of one bond, they exhibit generally higher barriers than quasi-degenerate single proton transfers. Therefore, the finding of a smaller barrier in TTAA can be rationalized if we assume a concerted double proton transfer in porphycene, so that the two cases can no longer easily be compared.

Conclusions

In conclusion, we have presented ^{15}N and ^{2}H NMR relaxation data of TTAA which are dominated by dipolar ^{15}N–^{1}H and quadrupolar ^{2}H relaxation mechanisms caused by ultrafast proton and deuteron transfer processes. Thus, we were able for the first time to study kinetic H/D isotope effects of an ultrafast intramolecular proton transfer in the nano- to picosecond time scale by NMR-relaxometry. By a careful analysis of the isotropic ^{15}N NMR chemical shifts as a function of temperature we provided evidence for the reaction scheme of Fig. 1b. The gas phase degeneracy between the two *trans*-tautomers 1 and 2 and the two *cis*-tautomers 3 and 4 is lifted in the solid state by a combination of intra- and intermolecular interactions. An appropriate dipolar and quadrupolar relaxation theory was developed and used to convert the relaxation data into rate constants. Thus, evidence was obtained that the reaction step which influences most the relaxation corresponds to step $3 \rightleftarrows 2$. Furthermore, evidence was obtained that at low temperatures tunneling is the dominant reaction pathway of proton transfer in TTAA. The kinetic data obtained are analyzed in a preliminary way in terms of a modified one-dimensional Bell tunneling model, but may serve in the future for the development of better more dimensional reaction models.

Acknowledgements

This work was supported by the Deutsche Forschungsgemeinschaft, Bonn-Bad Godesberg and the Fonds der Chemischen Industrie, Frankfurt.

Appendix

Firstly, we consider the relaxation of ^{15}N nuclei in TTAA exhibiting a reaction network depicted in Fig. 1b. We confine the treatment to a three-state case as form 4 cannot be observed experimentally. In particular, we focus on the case of an isotropic dipolar ^{15}N–^{1}H relaxation mechanism. For both types of nuclei, the spectral density functions can be calculated as

$$J^m(\omega_i) = \int_{-\infty}^{+\infty} \langle F^m(t) F^{m*}(t+\tau)\rangle \exp(-i\omega_i \tau) d\tau \qquad (16)$$

where $m = 0$, 1 or 2 labels the multiple quantum order.

The quantities of autocorrelation functions $\langle F^m(t)F^{m*}(t+\tau)\rangle$ can be found as a sum of nine components:

$$\langle F^m(t)F^{m*}(t+\tau)\rangle = \sum_i \sum_f F_i^m f_f^{m*} P[f, i, (t)]P(i) \qquad (17)$$

Here m means the multiple quantum order of correlation functions 0, 1 and 2, i is the initial states 1, 2 and 3 and f the final states 1, 2 or 3. After powder averaging the products $|F_i^m F_f^{m*}|$

can be expressed as:

$$|F_i^m F_f^{m*}| = S^m(R)(i)R(f)0.5(3\cos^2\Theta_{if} - 1), \quad (18)$$

where $S^m = 4/5, 2/15, 8/15$ for zero, first and second order. $R(i)$ and $R(f)$ equals the dipolar coupling constant in the initial and final state given as

$$D = \gamma_I \gamma_S \hbar r_{SI}^{-3}(t) \quad (19)$$

for two spin 1/2 nuclei at a distance r_{SI}, and Θ_{if} is the angle between the major axis of the dipolar tensor in the initial and final state. $P(i)$ in eqn. (17) stands for the probability of being in state m at initial time t, the population of each state in thermal equilibrium given as

$$P(1) = (K_{13} + K_{12} + 1)^{-1} \quad (20)$$

$$P(2) = (K_{12}^{-1} + K_{23} + 1)^{-1} \quad (21)$$

$$P(3) = (K_{13}^{-1} + K_{23}^{-1} + 1)^{-1} \quad (22)$$

assuming that $P(1) + P(2) + P(3) = 1$ and that the system does not leave the equilibrium during the experiment. For calculation of the probabilities of being in state f at time $t + \tau$ after being in state i at time t the following equation can be introduced:

$$\frac{\mathrm{d}}{\mathrm{d}t}\begin{pmatrix} P(1) \\ P(2) \\ P(3) \end{pmatrix} = \begin{pmatrix} a_{11} & a_{12} & a_{13} \\ a_{21} & a_{22} & a_{23} \\ a_{31} & a_{32} & a_{33} \end{pmatrix}\begin{pmatrix} P(1) \\ P(2) \\ P(3) \end{pmatrix} \quad (23)$$

using the following simplifications:

$$a_{11} = (-k_{12} - k_{13}), \quad a_{12} = k_{21}, \quad a_{13} = k_{31},$$
$$a_{21} = k_{12}, \quad a_{22} = (-k_{21} - k_{23}), \quad a_{23} = k_{32},$$
$$a_{31} = k_{13}, \quad a_{32} = k_{23}, \quad a_{33} = (-k_{31} - k_{32}).$$

For the time dependent fluctuation between the different states the following exponential expressions holds:

$$P[f, i, (t)] = \sum_{i=1}^{3} C_i \chi_f^{\lambda_i} \exp(\lambda_i t) \quad (24)$$

with $i, f = 1$, 2 and 3 as the initial and final states and λ_1, λ_2, and λ_3 as the eigenvalues of the matrix in eqn. (23). The values of $\chi_f(\lambda)$, the χ_f value for the first, second and third eigenvalue are given as:

$$\chi_1(\lambda) = 1 \quad (25)$$

$$\chi_2(\lambda) = \frac{\begin{vmatrix} k_{12} + k_{13} + \lambda_n & k_{31} \\ -k_{12} & k_{32} \end{vmatrix}}{\begin{vmatrix} k_{21} & k_{31} \\ -k_{21} - k_{23} - \lambda_n & k_{32} \end{vmatrix}}, \quad (26)$$

$$\chi_3(\lambda) = \frac{\begin{vmatrix} k_{21} & k_{13} + k_{12} + \lambda_n \\ -k_{21} - k_{23} - \lambda_n & -k_{12} \end{vmatrix}}{\begin{vmatrix} k_{21} & k_{31} \\ -k_{21} - k_{23} - \lambda_n & k_{32} \end{vmatrix}}, \quad (27)$$

The prefactors in eqn. (24) can be calculated as

$$C_1(1) = \begin{vmatrix} 1 & \chi_2^{(1)} & \chi_3^{(1)} \\ 0 & \chi_2^{(2)} & \chi_3^{(2)} \\ 0 & \chi_2^{(3)} & \chi_3^{(3)} \end{vmatrix}/W, \quad (28)$$

$$C_1(2) = \begin{vmatrix} \chi_1^{(1)} & 1 & \chi_3^{(1)} \\ \chi_1^{(2)} & 0 & \chi_3^{(2)} \\ \chi_1^{(3)} & 0 & \chi_3^{(3)} \end{vmatrix}/W, \quad (29)$$

$$C_1(3) = \begin{vmatrix} \chi_1^{(1)} & \chi_2^{(1)} & 1 \\ \chi_1^{(2)} & \chi_2^{(2)} & 0 \\ \chi_1^{(3)} & \chi_2^{(3)} & 0 \end{vmatrix}/W, \quad (30)$$

$$C_2(1) = \begin{vmatrix} 0 & \chi_2^{(1)} & \chi_3^{(1)} \\ 1 & \chi_2^{(2)} & \chi_3^{(2)} \\ 0 & \chi_2^{(3)} & \chi_3^{(3)} \end{vmatrix}/W, \quad (31)$$

$$C_2(2) = \begin{vmatrix} \chi_1^{(1)} & 0 & \chi_3^{(1)} \\ \chi_1^{(2)} & 1 & \chi_3^{(2)} \\ \chi_1^{(3)} & 0 & \chi_3^{(3)} \end{vmatrix}/W, \quad (32)$$

$$C_2(3) = \begin{vmatrix} \chi_1^{(1)} & \chi_2^{(1)} & 0 \\ \chi_1^{(2)} & \chi_2^{(2)} & 1 \\ \chi_1^{(3)} & \chi_2^{(3)} & 0 \end{vmatrix}/W, \quad (33)$$

$$C_3(1) = \begin{vmatrix} 0 & \chi_2^{(1)} & \chi_3^{(1)} \\ 0 & \chi_2^{(2)} & \chi_3^{(2)} \\ 1 & \chi_2^{(3)} & \chi_3^{(3)} \end{vmatrix}/W, \quad (34)$$

$$C_3(2) = \begin{vmatrix} \chi_1^{(1)} & 0 & \chi_3^{(1)} \\ \chi_1^{(2)} & 0 & \chi_3^{(2)} \\ \chi_1^{(3)} & 1 & \chi_3^{(3)} \end{vmatrix}/W, \quad (35)$$

$$C_3(3) = \begin{vmatrix} \chi_1^{(1)} & \chi_2^{(1)} & 0 \\ \chi_1^{(2)} & \chi_2^{(2)} & 0 \\ \chi_1^{(3)} & \chi_2^{(3)} & 1 \end{vmatrix}/W, \quad (36)$$

with

$$W = \begin{vmatrix} \chi_1^{(1)} & \chi_2^{(1)} & X_3^{(1)} \\ \chi_1^{(2)} & \chi_2^{(2)} & \chi_3^{(2)} \\ \chi_1^{(3)} & \chi_2^{(3)} & \chi_3^{(3)} \end{vmatrix}/W, \quad (37)$$

Putting things together leads to the overall correlation function for a triple minimum potential:

$$\begin{aligned}
&\langle F^m(t)F^{m*}(t+\tau)\rangle = \\
&F_1^m F_1^m[C_1(1)\chi_1(\lambda_1)\exp(\lambda_1 t) + C_2(1)\chi_1(\lambda_2)\exp)\lambda_2 t) \\
&+ C_3(1)\chi_1(\lambda_3)\exp(\lambda_3 t)]P(1) + F_1^m F_2^m[C_1(1)\chi_2(\lambda_1)\exp(\lambda_1 t) \\
&+ C_2(1)\chi_2(\lambda_2)\exp(\lambda_2 t) + C_3(1)\chi_2(\lambda_3)\exp(\lambda_3 t)]P(1) \\
&+ F_1^m F_3^m[C_1(1)\chi_3(\lambda_1)\exp(\lambda_1 t) + C_2(1)\chi_3(\lambda_2)\exp(\lambda_2 t) \\
&+ C_3(1)\chi_3(\lambda_3)\exp(\lambda_3 t)]P(1) + F_2^m F_1^m[C_1(2)\chi_1(\lambda_1)\exp(\lambda_1 t) \\
&+ C_2(2)\chi_1(\lambda_2)\exp(\lambda_2 t) + C_3(2)\chi_1(\lambda_3)\exp(\lambda_3 t)]P(2) \\
&+ F_2^m F_2^m[C_1(2)\chi_2(\lambda_1)\exp(\lambda_1 t) + C_2(2)\chi_2(\lambda_2)\exp(\lambda_2 t) \\
&+ C_3(2)\chi_2(\lambda_3)\exp(\lambda_3 t)]P(2) + F_2^m F_3^m[C_1(2)\chi_3(\lambda_1)\exp(\lambda_1 t) \\
&+ C_2(2)\chi_3(\lambda_2)\exp(\lambda_2 t) + C_3(2)\chi_3(\lambda_3)\exp(\lambda_3 t)]P(2) \\
&+ F_3^m F_1^m[C_1(3)\chi_1(\lambda_1)\exp(\lambda_1 t) + C_2(3)\chi_1(\lambda_2)\exp(\lambda_2 t) \\
&+ C_3(3)\chi_1(\lambda_3)\exp(\lambda_3 t)]P(3) + F_3^m F_2^m[C_1(3)\chi_2(\lambda_1)\exp(\lambda_1 t) \\
&+ C_2(3)\chi_2(\lambda_2)\exp(\lambda_2 t) + C_3(3)\chi_2(\lambda_3)\exp(\lambda_3 t)]P(3) \\
&+ F_3^m F_3^m[C_1(3)\chi_3(\lambda_1)\exp(\lambda_1 t) + C_2(3)\chi_3(\lambda_2)\exp(\lambda_2 t) \\
&+ C_3(3)\chi_3(\lambda_3)\exp(\lambda_3 t)]P(3). \quad (38)
\end{aligned}$$

or rewritten as

$$\langle F^m(t)F^{m*}(t+\tau)\rangle = A^m \exp(\lambda_1 t) + B^m \exp(\lambda_2 t) + C^m \exp(\lambda_3 t) \quad (39)$$

with

$$A^m = P(1)(F_1^m F_1^m C_1(1)\chi_1(\lambda_1) + F_1^m F_2^m C_1(1)\chi_2(\lambda_1) + F_1^m F_3^m C_1(1)\chi_3(\lambda_1)) + P(2)(F_2^m F_1^m C_1(2)\chi_1(\lambda_1) + F_2^m F_2^m C_1(2)\chi_2(\lambda_1) + F_2^m F_3^m C_1(2)\chi_3(\lambda_1)) + P(3)(F_3^m F_1^m C_1(3)\chi_1(\lambda_1) + F_3^m F_2^m C_1(3)\chi_2(\lambda_1) + F_3^m F_3^m C_1(3)\chi_3(\lambda_1)) \quad (40)$$

$$B^m = P(1)(F_1^m F_1^m C_1(1)\chi_1(\lambda_2) + F_1^m F_2^m C_1(1)\chi_2(\lambda_2) + F_1^m F_3^m C_1(1)\chi_3(\lambda_2)) + P(2)(F_2^m F_1^m C_1(2)\chi_1(\lambda_2) + F_2^m F_2^m C_1(2)\chi_2(\lambda_2) + F_2^m F_3^m C_1(2)\chi_3(\lambda_2)) + P(3)(F_3^m F_1^m C_1(3)\chi_1(\lambda_2) + F_3^m F_2^m C_1(3)\chi_2(\lambda_2 + F_3^m F_3^m C_1(3)\chi_3(\lambda_2)) \quad (41)$$

$$C^m = P(1)(F_1^m F_1^m C_1(1)\chi_1(\lambda_3) + F_1^m F_2^m C_1(1)\chi_2(\lambda_3) + F_1^m F_3^m (C_1(1)\chi_3(\lambda_3)) + P(2)(F_2^m F_1^m C_1(2)\chi_1(\lambda_3) + F_2^m F_2^m C_1(2)\chi_2(\lambda_3) + F_2^m F_3^m C_1(2)\chi_3(\lambda_3)) + P(3)(F_3^m F_1^m C_1(3)\chi_1(\lambda_3) + F_3^m F_2^m C_1(3)\chi_2(\lambda_3) + F_3^m F_3^m C_1(3)\chi_3(\lambda_3)) \quad (42)$$

Because $\lambda_1 = 0$, the spectral densities for a triple minimum potential can be expressed by the Fourier transform of the correlation function:

$$J^m(\omega_I) = B^m \frac{2\tau_b}{1 + \omega_I^2\tau_b^2} + C^m \frac{2\tau_c}{1 + \omega_I^2\tau_c^2} \quad (43)$$

introducing the two correlation times

$$\frac{1}{\tau_b} = -\lambda_2, \quad (44)$$

$$\frac{1}{\tau_c} = -\lambda_3 \quad (45)$$

For the isotropic relaxation time of a spin S caused by dipolar interaction to a moving (during relaxation period non-radiated) nucleus I, the following master equation was developed elsewhere[1,18–20] (compare eqn. (1) in text)

$$\frac{1}{T_{1S}} = (\mu_0/4\pi)^2 S(S+1) \times [\tfrac{1}{12}J^{(0)}(\omega_1 - \omega_S) + \tfrac{3}{2}J^{(1)}(\omega_S) + \tfrac{3}{4}J^{(2)}(\omega_I + \omega_S)] \quad (46)$$

which can be transformed for our case using eqn. (43) into

$$\frac{1}{T_{1S}} = (\mu_0/4\pi)^2 \frac{2}{15} S(S+1) \frac{N_I}{N_S^2} \times \sum_S \sum_I \{[X_2\, g(\tau_b) + X_3\, g(\tau_c)]\} \quad (47)$$

where N_S represents the number of spins S (for example ^{15}N) and N_I the number of spins I belonging to vector r_{SI} participating in motion (usually ^{1}H). The prefactors X_2 and X_3 are the sums over B^m and C^m for the different quantum orders $m = 1$, 2, and 3. The functions $g(\tau)$ are given as

$$g(\tau) = \frac{\tau}{1 + (\omega_I - \omega_S)^2\tau^2} + \frac{3\tau}{1 + \omega_S{}^2\tau^2} + \frac{6\tau}{1 + (\omega_I + \omega_S)^2\tau^2} \quad (48)$$

For easier computation the correlation times can be calculated according to Latanowicz *et al.*[10] using

$$\tau_b = (J + Q)/2 \quad (49)$$

$$\tau_c = (J - Q)/2 \quad (50)$$

with

$$J = k_{13} + k_{31} + k_{23} + k_{32} + k_{12} + k_{21}, \quad (51)$$

$$Q = [J^2 - 4(k_{13}k_{32} + k_{23}k_{31} + k_{13}k_{23} + k_{23}k_{12} + k_{21}k_{31} + k_{21}k_{32} + k_{21}k_{13} + k_{12}k_{31} + k_{12}k_{32})]^{1/2} \quad (52)$$

The factors X_2 and X_3 can be expressed by

$$X_2 = C_2(1)P(1)G_1 + C_2(2)P(2)G_2 + C_2(3)P(3)G_3 \quad (53)$$

$$X_3 = C_3(1)P(1)G_1 + C_3(2)P(2)G_2 + C_3(3)P(3)G_3, \quad (54)$$

introducing three geometrical factors G_1, G_2 and G_3 including the geometric dependencies of the dipolar (or quadrupolar, in the case of ^{2}H) coupling. The factors can be represented by

$$G_1 = \chi_1(1)R(1)R(1) + 0.5\chi_2(1)R(1)R(2)(3\cos^2\theta_{12} - 1) + 0.5\chi_3(1)R(1)R(3)(3\cos^2\theta_{13} - 1), \quad (55)$$

$$G_2 = 0.5\chi_1(2)R(2)(3\cos^2\theta_{12} - 1) + \chi_2(2)R(2)R(2) + 0.5\chi_3(2)R(2)R(3)(3\cos^2\theta_{23} - 1), \quad (56)$$

$$G_3 = 0.5\chi_1(3)R(1)R(3)(3\cos^2\theta_{13} - 1) + 0.5\chi_3(3)R(2)R(3)(3\cos^2\theta_{23} - 1) + \chi_2(3)R(3)R(3). \quad (57)$$

$R(1)$, $R(2)$ and $R(3)$ equal the dipolar coupling constant D of eqn. (3) at different states 1, 2 and 3, θ_{12}, θ_{13} and θ_{23} are the jump angles between the direction of D in the two configurations shown in Fig. 2 as jump angle α. For the case of quadrupolar relaxation $R(1)$, $R(2)$ and $R(3)$ equals the quadrupolar coupling tensor $q$cc and θ_{rs} the jump angle between the two main axes of the quadrupolar coupling tensor.

References

1 B. H. Meier, F. Graf and R. R. Ernst, *J. Chem. Phys.*, 1982, **76**, 767.

2 (*a*) S. Nagaoka, F. Terao, F. Imaschiro, A. Saika and N. J. Hirota, *Chem. Phys.*, 1983, **79**, 4694; (*b*) N. Imaoka, S. Takeda and H. Chihara, *Bull. Chem. Soc. Jpn.*, 1988, **61**, 1865; (*c*) T. Inabe, I. Luneau, T. Mitani, Y. Maruyama and S. Takeda, *Bull. Chem. Soc. Jpn.*, 1994, **67**, 612; (*d*) S. Takeda, H. Chihara, T. Inabe, T. Mitani and Y. Marauyama, *Chem. Phys. Lett.*, 1992, **189**, 13.

3 (*a*) E. R. Andrew and L. Latanowicz, *J. Magn. Reson.*, 1986, **68**, 232; (*b*) L. Latanowicz and E. C. Reynhardt, *Ber. Bunsen-Ges. Phys. Chem.*, 1994, **98**, 818; (*c*) W. Medycki and S. Idziak, *Mol. Phys.*, 1995, **86**, 257; (*d*) L. Latanowicz, E. C. Reynhardt, R. Utrecht and W. Medycki, *Ber. Bunsen-Ges. Phys. Chem.*, 1995, **99**, 152; (*e*) E. C. Reynhardt and L. Latanowicz, *Chem. Phys. Lett.*, 1996, **251**, 235.

4 J. L. Skinner and H. P. Trommsdorff, *J. Chem. Phys.*, 1988, **89**, 897.

5 (*a*) A. J. Horsewill and A. J. Aibout, *J. Phys. Condens. Matter*, 1989, **1**, 9609; (*b*) A. J. Horsewill, A. Ikram and I. B. I. Tomash, *Mol. Phys.*, 1995, **84**, 1257.

6 E. C. Reynhardt, *Mol. Phys.*, 1992, **76**, 525.

7 J. Dolinsek, B. Zalar and R. Blinc, *Phys. Rev. B*, 1994, **50**, 805.

8 (*a*) S. Benz, U. Haeberlen and J. Tegenfeld, *J. Magn. Reson.*, 1986, **68**, 232; (*b*) A. Heuer and U. Haeberlen, *J. Chem. Phys.*, 1991, **95**, 4201.

9 (*a*) A. Stöckli, B. H. Meier, R. Kreis, R. Meyer and R. R. Ernst, *J. Chem. Phys.*, 1990, **93**, 1502; (*b*) R. Meyer and R. R. Ernst, *J. Chem. Phys.*, 1990, **93**, 5518; (*c*) R. Meier and R. R. Ernst, *J. Chem. Phys.*, 1990, **93**, 3437.

10 (*a*) L. Latanowicz and Z. Pajak, *Ber. Bunsen-Ges. Phys. Chem.*, 1989, **93**, 1440; (*b*) E. Knop, L. Latanowicz and E. C. Reynhardt, *Ber. Bunsen-Ges. Phys. Chem.*, 1993, **97**, 1457; (*c*) L. Latanowicz and Z. Pajak, *Mol. Phys.*, 1994, **82**, 1187; (*d*) L. Latanowicz, E. C. Andrew and E. C. Reynhardt, *J. Magn. Reson.*, 1994, **107**, 194; (*e*) L. Latanowicz and E. C. Reynhardt, *J. Magn. Reson. A*, 1996, **121**, 23; (*f*) L. Latanowicz and E. C. Reynhardt, *Mol. Phys.*, 1997, **90**, 107; (*g*) E. C. Reynhardt and L. Latanowicz, *J. Magn. Reson.*, 1998, **130**, 195; (*h*) W. Medycki, E. C. Reynhardt and L. Latanowicz, *Mol. Phys.*, 1998, **93**, 323.

11 (*a*) H. H. Limbach, J. Hennig, R. D. Kendrick and C. S. Yannoni, *J. Am. Chem. Soc.*, 1984, **106**, 4059; (*b*) B. Wehrle, H. H. Limbach, M. Köcher, O. Ermer and E. Vogel, *Angew. Chem.*, 1987, **99**, 914; B. Wehrle, H. H. Limbach, M. Köcher, O. Ermer and E. Vogel, *Angew. Chem., Int. Ed. Engl.*, 1987, **26**, 934; (*c*) B. Wehrle and

H. H. Limbach, *Chem. Phys.*, 1989, **136**, 223; (*d*) J. Braun, M. Schlabach, B. Wehrle, M. Köcher, E. Vogel and H. H. Limbach, *J. Am. Chem. Soc.*, 1994, **116**, 6593; (*e*) J. Braun, R. Schwesinger, P. G. Williams, H. Morimoto, D. E. Wemmer and H. H. Limbach, *J. Am. Chem. Soc.*, 1996, **118**, 11101.
12 H. H. Limbach, B. Wehrle, M. Schlabach, R. Kendrick and C. S. Yannoni, *J. Magn. Reson.*, 1988, **77**, 84.
13 (*a*) F. Aguilar-Parrilla, O. Klein, J. Elguero and H. H. Limbach, *Ber. Bunsen-Ges. Phys. Chem.*, 1997, **101**, 884; (*b*) R. Anulewicz, I. Wawer, T. M. Krygowski, F. Männle and H. H. Limbach, *J. Am. Chem. Soc.*, 1997, **119**, 12223; (*c*) F. Männle, I. Wawer and H. H. Limbach, *Chem. Phys. Lett.*, 1996, **256**, 657.
14 (*a*) H. H. Limbach, B. Wehrle, H. Zimmermann, R. Kendrick and C. S. Yannoni, *Angew. Chem.*, 1987, **99**, 241; H. H. Limbach, B. Wehrle, H. Zimmermann, R. Kendrick and C. S. Yannoni, *Angew. Chem. Int. Ed. Engl.*, 1987, **26**, 247; (*b*) H. H. Limbach, B. Wehrle, H. Zimmermann, R. Kendrick and C. S. Yannoni, *J. Am. Chem. Soc.*, 1987, **109**, 929; (*c*) B. Wehrle, H. Zimmermann and H. H. Limbach, *J. Am. Chem. Soc.*, 1988, **110**, 7014; (*d*) B. Wehrle, F. Aguilar-Parrilla and H. H. Limbach, *J. Magn. Reson.*, 1990, **87**, 584; (*e*) F. Aguilar-Parrilla, B. Wehrle, H. Bräunling and H. H. Limbach, *J. Magn. Reson.*, 1990, **87**, 592; (*f*) C. Benedict, U Langer, H. H. Limbach, H. Ogata and S. Takeda, *Ber. Bunsen-Ges. Phys. Chem.*, 1998, **102**, 335.
15 (*a*) C. G. Hoelger, B. Wehrle, H. Benedict and H. H. Limbach, *J. Phys. Chem.*, 1994, 98, 843; (*b*) S. Takeda, T. Inabe, C. Benedict, U. Langer and H. H. Limbach, *Ber. Bunsen-Ges. Phys. Chem.*, 1998, **102**, 1358; (*c*) U. Langer, Ch. Hoelger, B. Wehrle, L. Latanowicz, E. Vogel and H. H. Limbach, *J. Phys. Org. Chem.*, 2000, **13**, 23.
16 V. L. Goedken, J. J. Pluth, S. M. Peng Shie-Ming and B. Bursten, *J. Am. Chem. Soc.*, 1976, **98**, 8014.
17 (*a*) T. Butenhoff and C. B. Moore, *J. Am. Chem. Soc.*, 1988, **110**, 8336; (*b*) T. Butenhoff, R. S. Chuck, H. H. Limbach and C. B. Moore, *J. Phys. Chem.*, 1990, **94**, 7847.
18 A. Abragam, *Principles of Nuclear Magnetism*, Oxford University, New York, 1961.
19 M. Mehring, in *NMR—Basic Principles and Progress*, Springer-Verlag, Berlin, 1976, vol. 11.
20 H. W. Spiess, in *NMR—Basic Principles and Progress*, Springer-Verlag, Berlin, 1978, vol. 15, p. 55.
21 H. H. Limbach, B. Wehrle, M. Schlabach, R. Kendrick and C. S. Yannoni, *J. Magn. Reson.*, 1988, **77**, 84.
22 D. A. J. Torchia, *J. Magn. Reson.*, 1978, **30**, 613.
23 P. Du Bois Murphy, *J. Magn. Reson.*, 1986, **70**, 307.
24 K. N. Trueblood, in *Accurate Molecular Structures; their Determination and Importance*, ed. A. Domenicano and I. Hargittai, Oxford University Press, 1992, ch. 8, p. 200.
25 C. G. Hoelger and H. H. Limbach, *J. Phys. Chem.*, 1994, **98**, 11803.
26 Th. Steiner, *J. Chem. Soc., Chem. Commun.*, 1995, 1331.
27 (*a*) H. Benedict, C. Hoelger, F. Aguilar-Parrilla, W. P. Fehlhammer, M. Wehlan, R. Janoschek and H. H. Limbach, *J. Mol. Struct.*, 1996, **378**, 11; (*b*) H. Benedict, H. H. Limbach, M. Wehlan, W. P. Fehlhammer, N. S. Golubev and R. Janoschek, *J. Am. Chem. Soc.*, 1998, **120**, 2939; (*c*) M. Ramos, I. Alkorta, J. Elguero, N. S. Golubev, G. S. Denisov, H. Benedict and H. H. Limbach, *J. Phys. Chem. A*, 1997, **101**, 9791.
28 R. P. Bell, *The Tunnel Effect*, Chapman and Hall, London, 2nd edn., 1980.